

Long-term monitoring of ground anchor tensile forces by FBG sensors embedded tendon

Hyun-Jong Sung^a, Tan Manh Do^b, Jae-Min Kim^c and Young-Sang Kim*

Department of Civil and Environmental Engineering, Chonnam National University, Yeosu 550-749, Korean

(Received July 10, 2015, Revised July 16, 2016, Accepted July 25, 2016)

Abstract. Recently, there has been significant interest in structural health monitoring for civil engineering applications. In this research, a specially designed tendon, proposed by embedding FBG sensors into the center king cable of a 7-wire strand tendon, was applied for long-term health monitoring of tensile forces on a ground anchor. To make temperature independent sensors, the effective temperature compensation of FBG sensors must be considered. The temperature sensitivity coefficient β' of the FBG sensors embedded tendon was successfully determined to be $2.0 \times 10^{-5} \text{ } ^\circ\text{C}^{-1}$ through calibrated tests in both a model rock body and a laboratory heat chamber. Furthermore, the obtained result for β' was formally verified through the ground temperature measurement test, expectedly. As a result, the ground temperature measured by a thermometer showed good agreement compared to that measured by the proposed FBG sensor, which was calibrated considering to the temperature sensitivity coefficient β' . Finally, four prototype ground anchors including two tension ground anchors and two compression ground anchors made by replacing a tendon with the proposed smart tendon were installed into an actual slope at the Yeosu site. Tensile forces, after temperature compensation was taken into account using the verified temperature sensitivity coefficient β' and ground temperature obtained from the Korean Meteorological Administration (KMA) have been monitored for over one year, and the results were very consistent to those measured from the load cell, interestingly.

Keywords: effective temperature compensation; FBG sensors; long-term monitoring; ground anchor tensile force

1. Introduction

Unlike conventional electromechanical sensors such as Tensmeg, electrical strain gauge or vibrating wire strain gauge (VWSG) are not only subject to long-term risk but also suffer from noise during long distance transmission despite their immunity to electromagnetic interference (EMI). Alternatively, fiber optic sensors (FOSs) have historically proven to be a reliable sensing element for the measurement of various physical, chemical, and biological parameters owing to their characteristics of relatively low weight, EMI immunity, and multiplexing capability (Udd 1995).

Among FOSs, fiber Bragg grating sensors (FBGs), a recently developed product, are the most commonly used sensors for monitoring civil infra-structures. One reason for this popularity is that the inherent self-referencing capability of FBGs, which is not affected by fluctuations in the light source intensity, enables a high degree of serial multiplexing along the length of a fiber (Meissner *et al.*

1997, Inaudi 2000, Calvert and Mooney 2004, Ren *et al.* 2004, Kesavan *et al.* 2005, Li *et al.* 2005, Talebinejad *et al.* 2009, Kim *et al.* 2011). Furthermore, FBGs can measure multiple parameters such as strain, temperature, displacement, pressure, or acceleration and offer absolute measurements with excellent resolution and range.

The possibility of using FBGs as a monitoring technique was investigated in the past throughout a variety of approaches including both field and laboratory tests. Schroeck *et al.* (2000) monitored strain in steel rock bolts using FBG sensor arrays and extended the measuring range of their FBGs to allow for measurements of up to 20% relative strain by designing special arrangements of FBGs. Cornelia *et al.* (2003) performed strain measurements with FBGs for in situ pile loading tests. A fiber Bragg grating (FBG) sensor network was installed into a large diameter concrete pile on a real construction site. The intention was to monitor its deformation behavior during several quasi-static loading cycles. The results of their tests showed that a comparison between the results of FBGs and conventional concrete strain gages (CSG) showed excellent correspondence. Lee *et al.* (2004) conducted a series of laboratory and field tests to evaluate the applicability of an optical fiber sensor system in the instrumentation of piles. The distributions of axial load in three model piles and a field test pile determined from the strains measured by FBGs were found to be comparable, in terms of both magnitude and trend, with those obtained from conventional strain gauges. Moerman *et al.* (2005) measured ground anchor forces of a quay wall with Bragg sensors. More recently, Kim *et al.* (2011) proposed the short-term

*Corresponding author, Professor

E-mail: geoykskim@jnu.ac.kr

^aPh.D.

E-mail: kysung0302@hanmail.net

^bPh.D. Student

E-mail: geotmdo@gmail.com

^cProfessor

E-mail: jm4kim@jnu.ac.kr

monitoring methodology of tension force and load transfer on a ground anchor by using optical FBG sensors embedded tendon. By comparing the pre-stress forces measured by the smart tendon and load cell, they found that the pre-stress force monitored with the FBG sensor located at the free part is comparable to that measured from the conventional load cell. Furthermore, the load transfer of pre-stressing force at the tendon-grout interface was successfully measured with FBGs distributed along the fixed part.

In addition to strain (used to determine force), temperature monitoring using FBGs has been addressed. Ren *et al.* (2004) successfully utilized FBGs to measure the temperature variation of soil and the thermal differences in a circulating water system. Dewynter *et al.* (2005) installed FBGs into multiple boreholes surrounding a central heating borehole to conduct in situ thermal measurements of argillaceous rocks. The results from the FBGs matched those from conventional resistive probes to within 0.2°C.

The literature reviewed above clearly indicates the suitability of using FBGs for monitoring constructions in harsh environments. However, most of these studies have either focused on short-term monitoring or solely strain or temperature measurements. FBGs are sensitive to both strain and temperature, because the Bragg wavelength changes in response to both strain and temperature variations, with the wavelength shift induced by a 1°C change in temperature being almost equivalent to that induced by 10 $\mu\epsilon$ of strain; therefore, temperature compensation is required for accurate long-term measurements. Thus, in order to use FBGs for long-term monitoring of the tensile force on a ground anchor, effective temperature compensation for FBG sensors was considered to make temperature independent sensors.

In this study, the temperature sensitivity coefficient β' of FBG sensors embedded tendon was successfully determined through calibrated tests in both a model rock body and a laboratory heat chamber. Finally, the tensile forces on a ground anchor installed at the Yeosu site after temperature compensation was taken into account using the verified temperature sensitivity coefficient β' and ground temperature obtained from the Korean Meteorological Administration (KMA) have been monitored for over one year.

2. Strain measurement principle of FBG sensors embedded tendon and its effective temperature compensation

2.1 Strain measurement principle of FBG sensors embedded tendon with a proper encapsulation technique

An FBG is a type of distributed Bragg reflector constructed in a short segment of optical fiber that reflects particular wavelengths of light and transmits all others. This effect is achieved by creating a periodic variation in the refractive index of the fiber core, which generates a wavelength-specific dielectric mirror. An FBG can therefore be used as an inline optical filter to block certain wavelengths or as a wavelength-specific reflector according

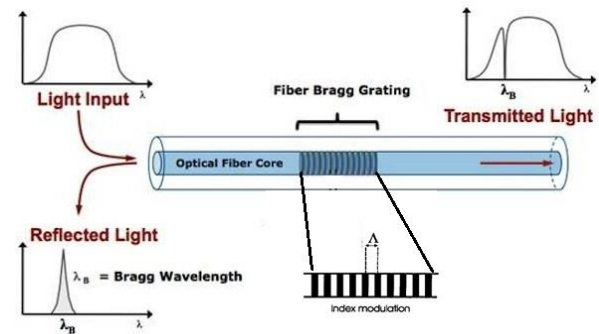


Fig. 1 Transmission and reflection spectra of FBG

to Gupta (2006).

When a light source with a broadband wavelength spectrum is inserted into the optical fiber, the Bragg grating (BG) reflects light waves with a narrowband spectrum as shown in Fig. 1. This allows us to obtain a reflection spectrum that is only dependent on the amount of change at the grated region. The center wavelength of the reflected light, λ_B , varies with the refractive index of the optical fiber, n_{eff} , and the spacing between the grating planes (Kersey 1996), A , as follows

$$\lambda_B = 2A n_{eff} \quad (1)$$

The center wavelength ranges typically from 1510 nm to 1590 nm. Both the index of refraction and the pitch length of the spacing are independently affected by changes in strain and temperature. Thus the shift in center wavelength of the FBG, $\Delta\lambda_B$, induced by strain and temperature changes, respectively $\Delta\epsilon$ and ΔT , is given by Othonos and Kalli (1999)

$$\Delta\lambda_B = \lambda_B [(1 - P_e)\Delta\epsilon + (\alpha + \xi)\Delta T] \quad (2)$$

where P_e is an effective strain-optic constant (approximately 0.22 for silica), α is the thermal expansion coefficient of the fiber (approximately $0.55 \times 10^{-6} \text{ } ^\circ\text{C}^{-1}$ for silica), and ξ represents the thermos-optic coefficient (approximately $8.6 \times 10^{-6} \text{ } ^\circ\text{C}^{-1}$ for germania-doped silica-core fiber). It should be noted that the change in strain in Eq. (2) is purely a result of external actions excluding temperature change since the thermal strain is considered in the second term. Under the simultaneous perturbations of strain and temperature, a measurement technique utilizing two FBG sensors with different gratings can be employed, provided that two linear equations from Eq. (2), obtained for two different FBG sensors, can be solved.

For an adequately small temperature change ΔT , Eq. (2) can be rearranged into the following Eq. (3) for strain change, $\Delta\epsilon$, as follows

$$\Delta\epsilon = \frac{1}{(1 - P_e)} \frac{\Delta\lambda_B}{\lambda_B} \quad (3)$$

More generally, the strain change can be mathematically computed from Eq. (2) based on the shift of the center wavelength in the spectrum of a reflected light wave, if the temperature is known.

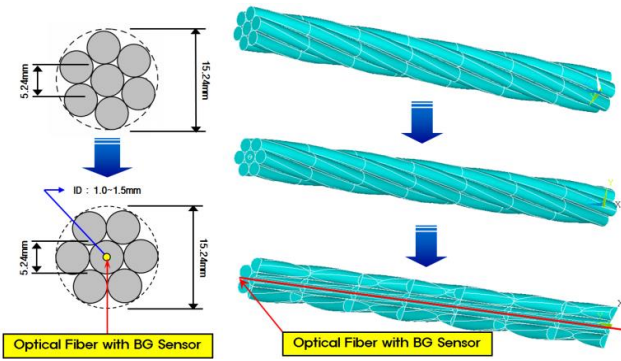


Fig. 2 Concept of a smart tendon (Kim *et al.* 2007, 2011)

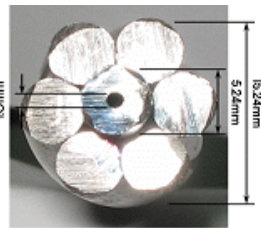


Fig. 3 Cross-section of a real smart tendon (Kim *et al.* 2007, 2011)

$$\Delta\varepsilon = \frac{\Delta\lambda_B}{\lambda_B} \frac{1}{(1-P_e)} - \frac{\beta' \Delta T}{(1-P_e)} \quad (4)$$

where $\beta'=(\alpha+\zeta)$ is the temperature sensitivity coefficient. In this study, an encapsulation method of optical fiber with BG sensors into a 7-wire strand is applied as shown in Fig. 2. This process takes advantage of the fact that the central steel wire of a 7-wire strand, called ‘king wire’, is straight, while the other six wires helically wrap the king wire. In order to encapsulate the FBG sensor into the tendon, we proposed the idea of replacing the king wire with a steel tube in which the optical fiber with FBG sensors is embedded. Since the diameter of a typical optical fiber is approximately 1/4 mm, a steel tube with an inside diameter of 2.0 mm or less is sufficient to accommodate the fiber and liquid glue (i.e., epoxy resin with low viscosity) (Kim *et al.* 2007, 2008, 2009, 2011). Fig. 3 shows a cross section of the tendon including a tube with an outer diameter of 5.24 mm and an inner diameter of 1.0~2.0 mm. The steel tube can easily be manufactured through the pultrusion process. The manufacturer working on the project is currently capable of extending its length up to 34.0 m, and the inside diameter of the steel tube ranges from 1.0 mm to 2.0 mm. The tube is usually made of mild steel for an easier pultrusion process, and then it is heat-treated to draw level with a higher tensile strength of pre-stressing tendon. Currently, the yield strength of the tube is typically 50% of the wire in the pre-stressing tendon, while that of the mild steel is approximately 1/3 of the high-strength wire. We expect that the strength of the tube can be further improved in the near future.

2.2 Temperature sensitivity coefficient of FBG sensors embedded tendon

For long-term monitoring of ground anchors using FBGs, owing to the considerable temperature change ΔT of the ground, sensor calibration of strain and temperature is required for obtaining accurate measurements. In this study, the calibration coefficient, namely, the temperature sensitivity coefficient β' of FBG sensors embedded tendon, was determined through calibrated tests in both a model rock body and a laboratory heat chamber.

2.2.1 Calibrated test in the model rock body

A 0.8 m length of smart tendon, where one FBG sensor and one thermometer are located at the same position, was manufactured as shown in Fig. 4. The tendon was affixed to the model rock body with grout to model the installation conditions of the ground anchor. The FBG sensor was used to measure the change of the reflected wavelength whereas the second device, a thermometer, responded to temperature variations. The test using a model rock body containing the proposed smart tendon was carried out in the laboratory as illustrated in Fig. 5. The temperature change ΔT of the model rock was observed to vary in the range of 2°C~12°C. Responding to the temperature change, the FBG sensor embedded tendon measured the change of the reflected wavelength.

As shown in the Fig. 6, a linear relationship exists between the temperature change and the change of the reflected wavelength.

Applying Eq. (4) to the current test, a solution for the temperature sensitivity coefficient β' can be found based on the initial conditions of the model test though the derived Eqs. (5) and (6).

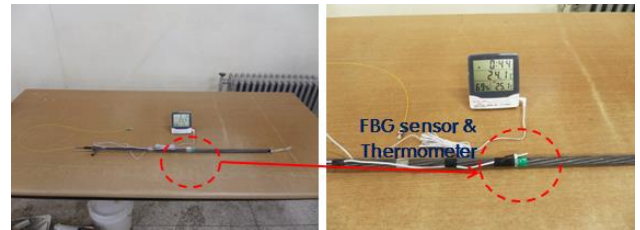


Fig. 4 Optical FBG sensors embedded in a 0.8 m long tendon



Fig. 5 Model rock body and monitoring devices

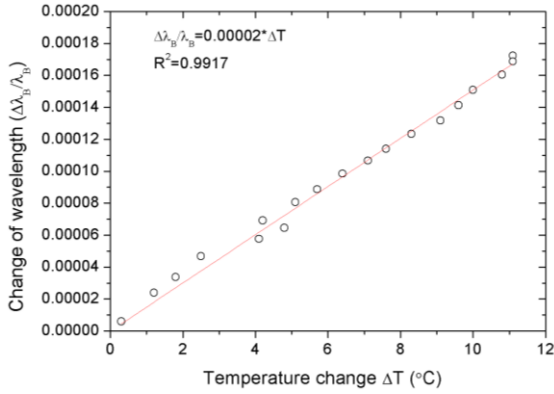


Fig. 6 Calibrated test result in the model rock body

$$0 = \frac{\Delta\lambda_B}{\lambda_B} \frac{1}{(1-P_e)} - \frac{\beta' \Delta T}{(1-P_e)} \quad (5)$$

$$\frac{\Delta\lambda_B}{\lambda_B} = \beta' \Delta T \quad (6)$$

The relationship observed in Fig. 6 was used to determine the temperature sensitivity coefficient β' ($\beta' = 2 \times 10^{-5} \text{ } ^\circ\text{C}^{-1}$) of the FBG sensor embedded tendon. The high R-Square value of 0.9917 indicated that an acceptably accurate calibration coefficient was obtained.

2.2.2 Calibrated test in the heat chamber

The same manufactured smart tendon with an FBG sensor and attached thermometer was used for the second calibrated test in the heat chamber. Figs. 7 and 8 show the procedure of the heat chamber test with a 0.5 m length of proposed smart tendon and other monitoring devices. Similar to the previous test, an FBG sensor was used to measure the change of the reflected wavelength, and the thermometer was used to measure temperature variation.

In this test, a higher temperature range of $10^\circ\text{C} \sim 40^\circ\text{C}$ was effectively generated by a heat chamber in the laboratory. During the testing process, time intervals of 30 min were maintained for every 10°C increment. As before, the temperature change measured by the thermometer is related to the change of the reflected wavelength measured by the FBG sensor. There was a considerable increase of the reflected wavelength when the temperature increased.

Similar to the calibrated test performed with the model rock body, a linear relationship between the temperature change and the change of the reflected wavelength was also discovered as shown in Fig. 9.

In order to determine the calibration coefficient, the same methodology as detailed in the previous test was systematically conducted using Eq. 4. Consistently, the obtained temperature sensitivity coefficient β' ($\beta' = 2 \times 10^{-5} \text{ } ^\circ\text{C}^{-1}$) was the same as that determined from the calibrated test in the model rock body. Therefore, for the proposed smart tendon with an embedded FBG sensor, the typical value of the temperature sensitivity coefficient β' is $2 \times 10^{-5} \text{ } ^\circ\text{C}^{-1}$.

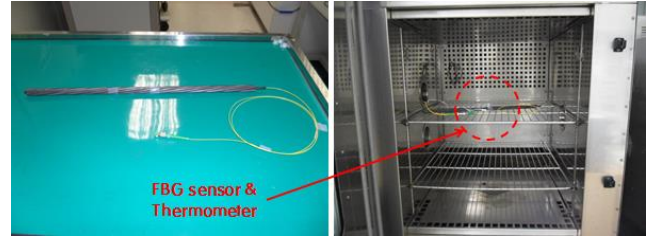


Fig. 7 Optical FBG sensors embedded within a 0.5 m long tendon

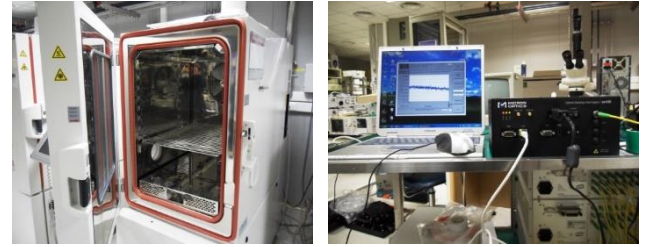


Fig. 8 Heat chamber and monitoring devices

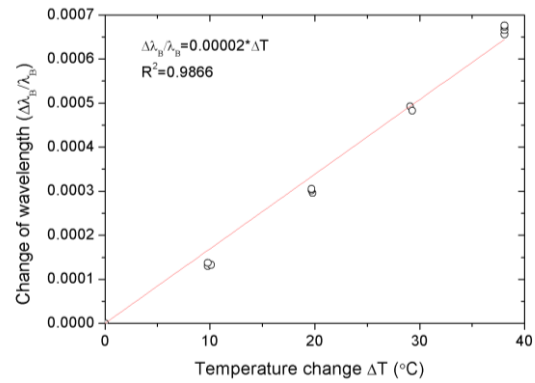


Fig. 9 Calibrated test result in the heat chamber

2.3 Validation of the temperature sensitivity coefficient for measuring ground temperature

For measuring ground temperature, an 11.5 m length of proto-type anchor, manufactured at the factory of Sam Woo Geotechnical Co. Ltd, was installed at the construction site of the Experimental Center for Coastal and Harbor Engineering (ECCHE) at Chonnam National University of Korea. In order to formally verify the temperature sensitivity coefficient β' of the FBG sensor in determining ground temperature, five FBG sensors were located in different positions of each tendon for this test as shown in Fig. 10. As previously mentioned, when FBG is affected by temperature, the changes of both periodicity and effective refraction index induced by temperature will result in a wavelength shift described in Eq. (4). Owing to a lack of strain on the tendon, the ground temperature change can be easily determined from the change of the reflected wavelength with the temperature sensitivity coefficient β' of the FBG sensors as indicated in Eq. (7).

$$\Delta T = \frac{1}{2 \times 10^{-5}} \times \frac{\Delta\lambda_B}{\lambda_B} \quad (7)$$

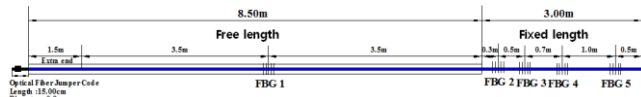


Fig. 10 FBG sensor array for measuring ground temperature



Fig. 11 Experiment setup for measuring ground temperature

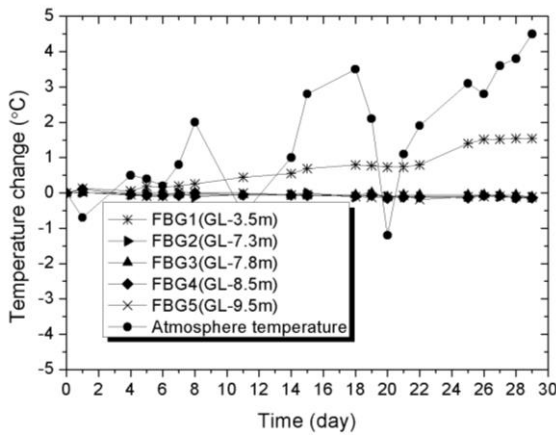


Fig. 12 Temperature change measured with FBGs

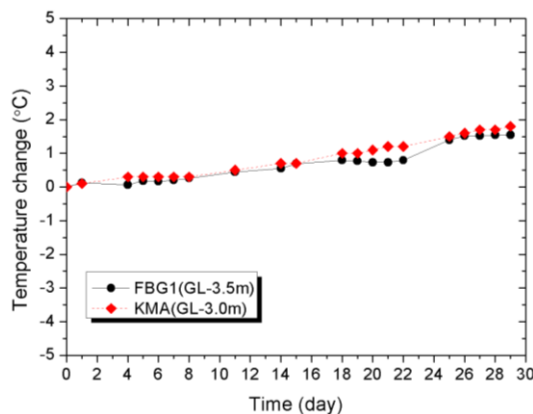


Fig. 13 Ground temperature changes from thermometer and FBG sensor(GL-3.0~3.5 m)

The ground temperature change was continuously monitored from June 16th 2011 to July 15th 2011. FBG1, which was located in the free part of the tendon, was used to measure the temperature change at a depth of 3.5 m from the ground surface. FBG2, FBG3, FBG4, and FBG5, which

were located in the fixed part of the tendon, recorded the temperatures at the depths of 7.3 m, 7.8 m, 8.5 m, and 9.5 m, respectively. The temperature changes determined from the FBGs during the monitored period are illustrated in Fig. 12. The atmospheric temperature variation is also indicated in Fig. 12.

Interestingly, the temperature variation measured by FBG1 is remarkably high when compared with those measured by FBG2, FBG3, FBG4 and FBG5. Thus, at depths greater than 7.3 m from the surface, there is almost no ground temperature change as shown in Fig. 12. Above that depth, near the surface, ground temperature is physically affected by atmosphere temperature. This is the explainable reason caused the change of shallow ground temperature during a period of time.

In addition, the KMA ground thermometer was also used to measure temperature change at a depth of 3 m (G.L.-3 m) during the one-month period. Fig. 13 shows both of the ground temperature changes measured by the ground thermometer and the FBG sensor (GL-3.0 ~ -3.5 m). Both devices indicate a very similar trend from beginning to end of the monitoring process with maximum observations of 1.8°C from the ground thermometer and 1.6°C from the FBG sensor. This finding is important when considering the validation of the temperature sensitivity coefficient β' for measuring ground temperature. Therefore, it can be concluded that the temperature sensitivity coefficient is valid for determining the ground temperature from the change of the reflected wavelength in FBG sensors.

3. Long-term monitoring of ground anchor tensile force with temperature compensation

3.1 Manufacturing of prototype anchors

For field applications, various types of ground anchors, including both tension type and compression type anchors, were tested with the usage of FBGs embedded smart tendons. Each step of the manufacturing process for FBGs embedded tendon is shown in Fig. 14. Ideally, this process takes advantage of the fact that the central steel wire of a 7-wire strand, called 'king wire', is straight, while the other six wires helically wrap the king wire.

In order to encapsulate the FBG sensor into the tendon, we proposed the idea of replacing the king wire with a steel tube in which the optical fiber with FBG sensors is embedded. Since the diameter of a typical optical fiber is approximately 1/4 mm, a steel tube with an inside diameter of 2.0 mm or less is sufficient to accommodate the fiber and liquid glue (i.e., epoxy resin with low viscosity) (Kim *et al.* 2011).

Two 11.2 m long tension-type anchors, named TA-1 and TA-2 together with 10.5 m long compression-type anchors named CA-1 and CA-2 were manufactured using the proposed smart tendons at the factory of Sam Woo Geotechnical Co. Ltd, which is a major company in the production of anchors in Korea. The manufacturing process of both tension-type and compression-type anchors at the factory are detailed in Figs. 15 and 16. The two

compression-type anchors were designed with the same dimensions of both free length and extra length. However, two tension-type anchors differed in their fixed lengths, which are the lengths usually used in geotechnical practice. In particular, anchors TA-1 and TA-2 were manufactured

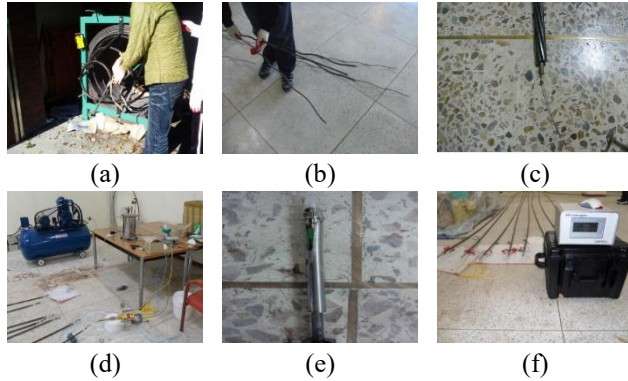


Fig. 14 Manufacturing process of FBG embedded tendon: (a) Cut the 7-wire strand, (b) Dismantle the strand and replace king cable, (c) Insert the optical fiber, (d) Insert the resin, (e) Protecting cap, (f) Test the FBG sensors

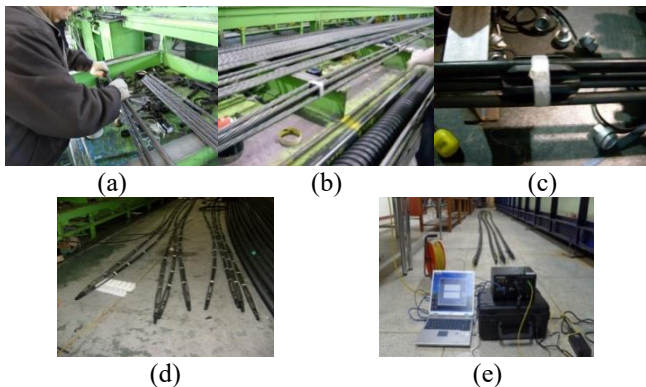


Fig. 15 Manufacturing tension anchors: (a) Cover the sheath, (b) Assemble tension anchors, (c) Fix the spacer, (d) Complete tension anchors, (e) Test FBG the sensors

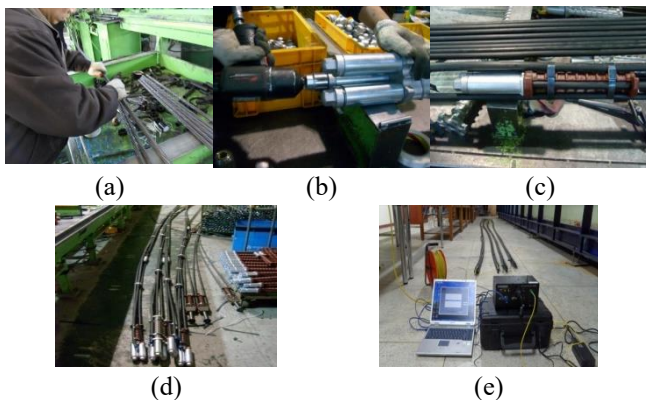


Fig. 16 Manufacturing compression anchors: (a) Cover the sheath, (b) Fix bearing plate anchors, (c) Assemble compression anchors, (d) Complete compression anchors, (e) Test the FBG sensors

Table 1 Initial wavelength and location of FBG Sensors arranged in ground anchors

No.	Initial Wavelength λ_B (nm)	Location of FBG sensor GL(-)m	FBG sensor dimension		Anchor Type
			Length (mm)	Diameter (mm)	
TA-1	λ_1 1528.0280	2.5	20	0.125	Tension
TA-2	λ_1 1552.0854	2.0			
CA-1	λ_1 1549.8637	7.1	20	0.125	Compression
	λ_2 1547.7299	9.1			
CA-2	λ_1 1555.9498	5.1	20	0.125	Compression
	λ_2 1557.7804	9.1			

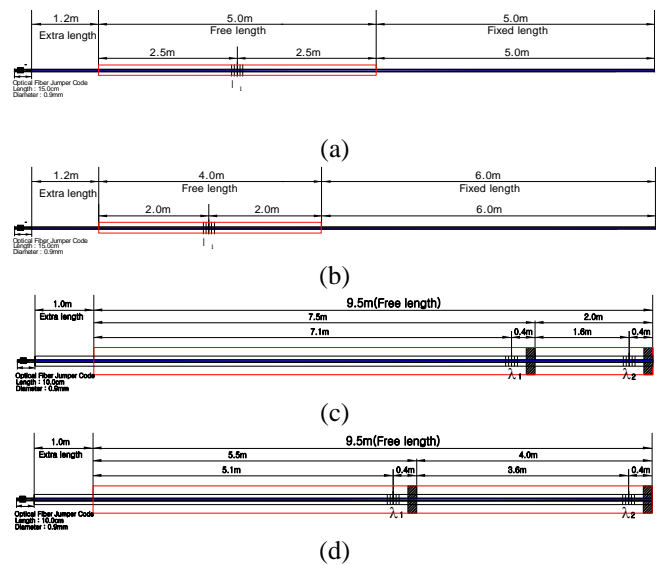


Fig. 17 Arrangement of FBG sensors in each anchor: (a) TA-1(Tension-type), (b) TA-2(Tension-type), (c) CA-1(Compression-type), (d) CA-2(Compression-type)

with 5.0 m and 6.0 m long fixed parts, respectively, whereas anchors CA-1 and CA-2 had the same free length of 9.5 m. Dimensions of the four anchors and design conditions are summarized in Table 2. In addition, the arrangement of the FBG sensors in each anchor TA-1, TA-2, CA-1, and CA-2 is shown in Fig. 17. The tension-type anchors were embedded with only one kind of FBG sensor, located at different positions; whereas two FBGs were embedded in each compression-type anchor. Each FBG sensor was produced to have a unique initial reflection wavelength within the 1528.03~1557.78 nm range, resulting in different wavelength shifts.

3.2 Installation and field test setup for long-term monitoring of the tensile force using FBGs

For long-term monitoring of the tensile force on ground anchors, tension-type and compression-type of ground anchors were installed at different construction sites of the Experimental Center for Coastal and Harbor Engineering (ECCHE) at Chonnam National University of Korea. The fixed lengths of the tension-type anchors were surrounded by soft rock conditions, while the compression-type anchors

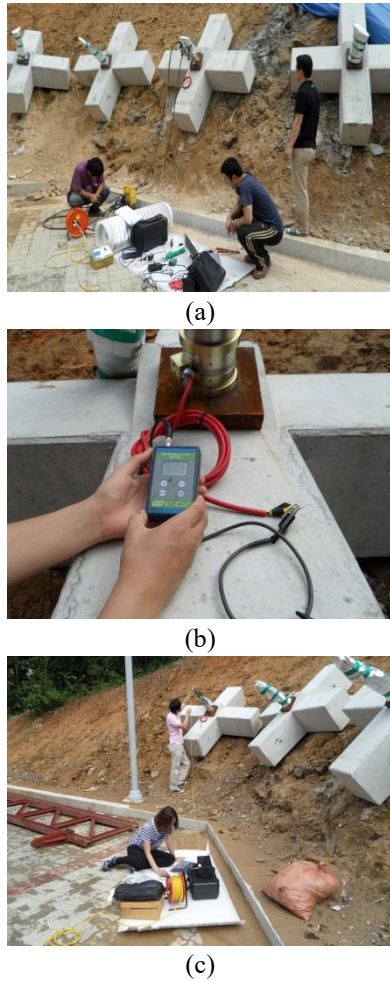


Fig. 18 Anchor measurement sequence for field test: (a) Initial jacking of anchor, (b) Load cell measurement, (c) FBG sensor measurement

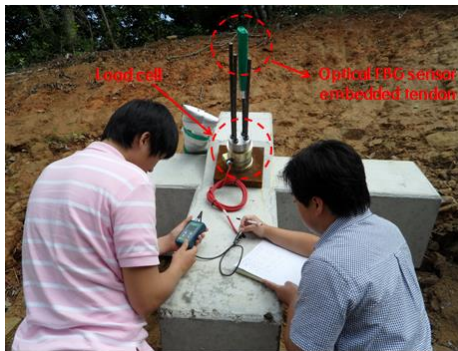


Fig. 19 Tensile force monitoring by using a load cell and an Optical FBG sensor simultaneously

Table 2 Dimensions of ground anchors and surrounding ground conditions for field tests

Anchor No.	Boring length (m)	Free length (m)	Fixed length (m)	Boring diameter (m)	Number of tendon (n)	Ground Condition	
TA-1	11.2	10.0	6.2	5.0	105	4	Soft Rock
TA-2			5.2	6.0	105	4	
CA-1	10.5	9.5	10.5	-	105	4	Weathered Rock ~ Soft Rock
CA-2			10.5	-	105	4	

with two bearing plates were fixed at weathered rock and soft rock conditions. Dimensions of the ground anchors and surrounding ground conditions for these field tests are summarized in detail in Table 2. Additionally, conventional load cells were also installed for the comparison. The anchor measurement sequences are illustrated in Figs. 18 and 19.

For the current methodology for long-term monitoring of the tensile force on ground anchors using FBGs, based on the principle of wavelength shifts, the FBG sensors were located in the free lengths of both anchor types to measure the tendon strains. The tensile forces were then directly estimated with Eq. (8) from the measured strain ϵ_{FBG}

$$P_{FBG} = N \cdot A_t \cdot E_t \cdot \epsilon_{FBG} \quad (8)$$

where P_{FBG} is the tensile force determined from the strain measured from the FBG; N is number of tendons in ground anchor; E_t is the Young's modulus of the tendon ($E_t=200$ GPa); A_t is the effective cross-sectional area of the tendon ($A_t=140$ mm²); ϵ_{FBG} is the strain measured from the first FBG sensor located in the free part.

3.3 Long term monitoring of tensile force by FBG sensors embedded tendon with temperature compensation

For the tension-type anchors, measurements were continuously monitored and recorded for a total period of more than one year. Figs. 20(a)-(b) show the atmospheric temperature and the ground temperature, which were recorded from the KMA. The anchor forces measured using the FBGs with and without temperature compensation were also plotted simultaneously. Since Kim *et al.* (2012) reported that tension forces measured from FBGs were comparable to high precision load cell within $\pm 5\%$, tensile forces measured by load cell were expressed as ranges of $\pm 5\%$ of measured value and used as a reference value.

During an approximately 13 month monitoring period, the atmospheric temperature ranged from -2.2°C to 28°C for both monitored cases of anchor TA-1 and TA-2, whereas the ground temperature of the TA-1 measured case (GL-3.0 m) and the TA-2 measured case (GL-1.5 m) ranged from 12.4°C to 20.6°C and 7.4°C to 24.2°C , respectively. The applied pre-stressing forces on anchors TA-1 and TA-2 were 215.96 kN and 149.37 kN, respectively. From Fig. 20(a)-(b), it is evident that the trends of the tensile forces before temperature compensation observed in both the TA-1 and TA-2 monitoring cases relatively conform to the corresponding ground temperature trends. It can be explained that the obtained tensile forces are influenced by ground temperatures before temperature compensation. Therefore, the temperature compensations are indispensable. And initial tensile force measured at TA-1 was close to +5% of that measured from load cell while initial tensile force of TA-2 was close to -5% of load cell measurement as reported Kim *et al.* (2012).

Even though there were little differences between initial tensile forces between FBGs and load cell, it may happen due to the slippage of wedge during setting of anchor head and may not be the practical problems for the purpose of

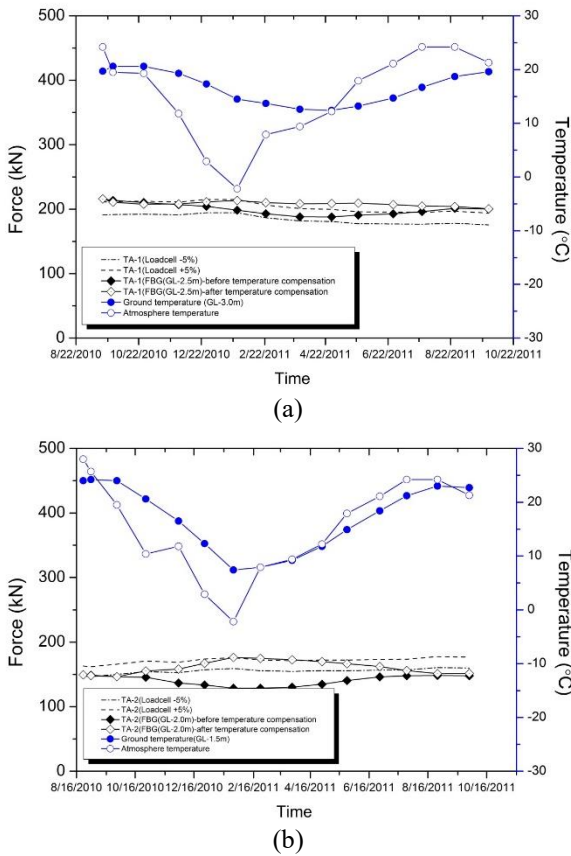


Fig. 20 Tensile force of ground anchors before and after temperature compensation: (a) TA-1, (b) TA-2

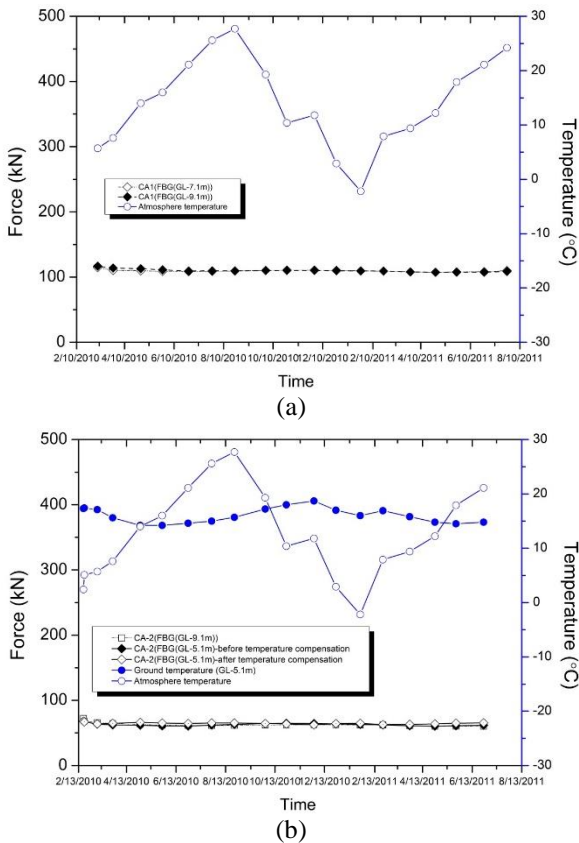


Fig. 21 Tensile force of ground anchors before and after temperature compensation: (a) CA-1, (b) CA-2

seasonal monitoring of tendon force. Expectedly, after temperature compensation with Eq. (4) and the temperature sensitivity coefficient β' ($\beta'=2 \times 10^{-5} \text{ } ^\circ\text{C}^{-1}$) of the FBG sensor embedded tendon, the tensile force measured by the FBG sensor looks independent of the ground temperature and comparable with the load cell measurement. To confirm the feasibility of temperature compensation by the proposed method, the correlation coefficient was calculated between tensile forces measured FBGs and load cell using Eq. (9) before and after temperature compensation. Correlation coefficient of TA-1 changes from 0.628 before compensation to 0.722 after compensation and that of TA-2 changes from -0.284 to 0.441. From the results, it is proven that the FBG sensors embedded tendon can be effectively applied to monitor the tensile force of ground anchor for long period with proposed temperature compensation method.

$$Correl(X, Y) = \frac{\sum(x - \bar{x})(y - \bar{y})}{\sqrt{\sum(x - \bar{x})^2 \sum(y - \bar{y})^2}} \quad (9)$$

Where x, y are the values of tensile forces measured by FBGs and load cell; \bar{x}, \bar{y} are the average values of tensile forces measured by FBGs and load cell, respectively.

Differing from the tension-type anchors, FBGs of the compression-type anchor were located deeply near bearing plates as summarized in Table 1 and shown in Fig. 17. For both compression anchors, the second FBG sensor was positioned at the same depth (GL-9.1 m), but the first FBG sensors of compression anchors CA-1 and CA-2 were positioned at different depths of GL-7.1 m and GL-5.1 m, respectively. Sensor location is mainly dependent on the ground condition and position of bearing plate.

As can be seen in Fig. 21(b), there was small ground temperature change at GL-5.1 m. And much less change is expected at the deeper location as shown in Fig. 12. Among FBG sensors of both compression anchors, only the first FBG sensor of anchor CA-2 positioned at the depth of GL-5.1 m needed compensation for the temperature change. A comparable trend was obtained in the result of compression-type anchor CA-2 at GL-5.1 m before and after temperature compensation. Therefore, we draw the conclusion that since ground temperature change is small in relatively deeper depth, temperature compensation has a slight effect on the FBG sensors in compression-type anchors. As expected in the measurements of the compression-type anchor CA-1, extremely small changes of the tensile force were monitored in the two FBG sensors located at GL-7.1 m and GL-9.1 m near bearing plates.

4. Conclusions

The long-term monitoring of ground anchor tensile forces were experimentally investigated by using FBG sensors embedded tendon. Based on the results, three main conclusions can be drawn as following:

The temperature sensitivity coefficient for the FBG sensor embedded tendon β' of $2 \times 10^{-5} \text{ } ^\circ\text{C}^{-1}$ was experimentally determined from the calibrated tests in both

a model rock body and a heat chamber test and was validated through field tests. Temperature changes measured from the FBG sensor embedded tendon matched those measured from the KMA.

For tension-type anchors, tensile forces were monitored by FBG sensors located relatively shallow depth for over one year and the results, after temperature compensation with β' and the ground temperature obtained from the KMA, were very consistent and comparable with those measured from the load cell. Therefore, it is feasible to compensate the temperature effect for the FBGs using ground temperatures measured by the Korean Meteorological Administration and the temperature sensitivity coefficient β' .

For compression-type anchors, FBG sensors are located relatively deep depth (generally deeper than GL-5.0 m) near load plate. Therefore temperature change was very limited and temperature compensation by proposed method affects slightly on tensile forces monitored by the FBG sensors embedded tendon. With or without temperature compensation, variation of the tensile forces is negligible.

Acknowledgments

This study was financially supported by Chonnam National University, 2011. The authors also thank J.Y. Kim, the President of Sam Woo Geotechnical Co. Ltd for his kind assistance in the manufacture and pullout test of the proto-type ground anchor.

References

- Calvert, S. and Mooney, J. (2004), "Bridge structural health monitoring system using fiber grating sensors: development and preparation for a permanent installation", *Proceedings of the SPIE 2004*.
- Cornelia, M., Schmidt-Hattenberger, Straub, T., Naumann, M., Borm, G., Lauerer, R., Beck, C. and Schwarz, W. (2003), "Strain measurements by fiber Bragg grating sensors for in situ pile loading tests", *Smart Sensor Technology and Measurement Systems*, 289.
- Dewynter, V., Rougeault, S., Boussoir, J., Roussel, N., Ferdinand, P. and Wileveau, Y. (2005), "Instrumentation of borehole with fiber Bragg grating thermal probes", *Int. Soc. Optic. Eng.*, **5855**, 1016-1019.
- Gupta, B.D. (2006), *Fiber Optic Sensors: Principles and Applications*, New India Publishing, New Delhi, ND, India.
- Inaudi, D. (2000), "Application of civil structural monitoring in Europe using fiber optic sensors", *Prog. Struct. Eng. Mat.*, **2**(3), 351-358.
- Kersey, A.D. (1996), "A review of recent developments in fiber optic sensor technology", *Optic. Fiber Technol.*, **2**(36), 291-317.
- Kesavan, K., Ravisankar, K., Parivallal, S. and Sreeshylam, P. (2005), "Applications of fiber optic sensors for structural health monitoring", *Smart Struct. Syst.*, **1**(4), 355-368.
- Kim, J.M., Kim, H.W., Park, Y.H., Yang, I.H. and Kim, Y.S. (2012), "FBG Sensors encapsulated into 7-wire steel strand for tension monitoring of a prestressing tendon", *Adv. Struct. Eng.*, **15**(6), 907-917.
- Kim, J.M., Kim, Y.S., Kim, H.W., Seo, D.N. and Yun, C.B. (2007), "Development of smart tendon instrumented with optical FBG sensors", *J. Comput. Struct. Eng. Inst. Korea*, **20**(2), 121.
- Kim, Y.S., Seo, D.N. and Kim, J.M. (2008), "Development and application of a smart anchor with optical FBG sensors", *Proceedings of KGS Spring National Conference 2008*, 393-398.
- Kim, Y.S., Seo, D.N., Kim, J.M. and Sung, H.J. (2009b), "Load transfer characteristics of the 7-wire strand using FBG sensor embedded smart tendon", *J. Korea Soc. Haz. Mitigation*, **9**(5), 79-86.
- Kim, Y.S., Sung, H.J., Kim, H.W. and Kim, J.M. (2011), "Monitoring of tension force and load transfer of ground anchor by using optical FBG sensors embedded tendon", *Smart Struct Syst.*, **7**(4), 303-317.
- Lee, W., Jin, Lee, W.Je., Lee, S.B. and Rodrigo, S. (2004), "Measurement of pile load transfer using the Fiber", *Can. Geotech. J.*, **41**(6), 1222-1232.
- Li, E., Xi, J., Chicharo, J., Liu, T., Li, X., Jiang, J., Li, L., Wang, Y. and Zhang, Y. (2005), "The experimental evaluation of FBG sensor for strain measurement of prestressed steel strand", *Proceedings of the SPIE*, **5649**.
- Meissner, J., Nowak, W., Slowik, V. and Klink, T. (1997), "Strain monitoring at a prestressed concrete bridge", *Proceedings of the Optical Fiber Sensors*, Williamsburg, Virginia, October.
- Moerman, W., Taerwe, L., Waele, W.D., Degrieck, J. and Himpe, J. (2005), "Measuring ground anchor forces of a quay wall with bragg sensors", *J. Struct. Eng.*, ASCE, **131**(2), 322-328.
- Othonos, A. and Kalli, K. (1999), *Fiber Bragg Gratings*, Artech House, London.
- Ren, L., Lee, H.N., Sun, L. and Lee, D.S. (2004), "FBG sensors for on-line temperature measurements", *Int. Soc. Optic. Eng.*, **5391**, 94-99.
- Ren, L., Li, N.H., Sun, L. and Li, D.S. (2005), "Development of tube-packaged FBG strain sensor and application in the vibration experiment of submarine pipeline model", *Proceedings of the SPIE 2005*, **5770**.
- Schroeck, M., Ecke, W. and Graupner, A. (2000), "Strain monitoring in steel rock bolts using FBG sensor arrays", *Appl. Optic. Fiber Sens.*, 289.
- Talebinejad, I., Fischer, C. and Ansari, F. (2009), "Serially multiplexed FBG accelerometer for structural health monitoring of bridges", *Smart Struct. Syst.*, **5**(4), 345-355.
- Udd, E. (1995), *Fiber Optic Smart Structure*, John Wiley & Sons, Inc.

CY